



PERGAMON

AVAILABLE AT  
www.ComputerScienceWeb.com

POWERED BY SCIENCE @ DIRECT®

Neural Networks 16 (2003) 121–132

Neural  
Networks

[www.elsevier.com/locate/neunet](http://www.elsevier.com/locate/neunet)

## Classification of clustered microcalcifications using a Shape Cognitron neural network

San-Kan Lee<sup>a,b</sup>, Pau-choo Chung<sup>c,\*</sup>, Chein-I Chang<sup>d</sup>, Chien-Shun Lo<sup>c</sup>,  
Tain Lee<sup>a</sup>, Giu-Cheng Hsu<sup>e</sup>, Chin-Wen Yang<sup>f</sup>

<sup>a</sup>Department of Radiology, Taichung Veterans General Hospital, VACRS, Taichung 40705, Taiwan, ROC

<sup>b</sup>Department of Diagnostic Radiology, National Defense Medical Center, Taipei 100, Taiwan, ROC

<sup>c</sup>Department of Electrical Engineering, National Cheng Kung University, Tainan 70101, Taiwan, ROC

<sup>d</sup>Remote Sensing Signal and Image Processing Laboratory, Department of Computer Science and Electrical Engineering,  
University of Maryland Baltimore County, Baltimore, MD 21250, USA

<sup>e</sup>Radiological Section, Taiwan Adventist Hospital, Taipei 40705, Taiwan, ROC

<sup>f</sup>Computer Center, Taichung Veterans General Hospital, VACRS, Taichung 40705, Taiwan, ROC

Received 30 June 2000; accepted 16 July 2002

### Abstract

A new shape recognition-based neural network built with universal feature planes, called Shape Cognitron (S-Cognitron) is introduced to classify clustered microcalcifications. The architecture of S-Cognitron consists of two modules and an extra layer, called *3D figure layer* lies in between. The first module contains a *shape orientation layer*, built with 20 cell planes of low level universal shape features to convert first-order shape orientations into numeric values, and a *complex layer*, to extract second-order shape features. The 3D figure layer is a feature extract-display layer that extracts the shape curvatures of an input pattern and displays them as a 3D figure. It is then followed by a second module made up of a feature formation layer and a probabilistic neural network-based classification layer. The system is evaluated by using Nijmegen mammogram database and experimental results show that sensitivity and specificity can reach 86.1 and 74.1%, respectively.

© 2002 Elsevier Science Ltd. All rights reserved.

**Keywords:** Microcalcifications classification; Neural networks; Shape Cognitron

### 1. Introduction

Microcalcifications (MCCs) generally present an early sign of breast cancer. According to related medical reports, although clustered MCCs associated with benign and malignant disease usually have distinct characteristics, studies involving a large number of cases also indicated that a considerable overlap exists. This creates diagnostic interpretation difficulty. Under such circumstance, most radiologists encourage biopsies, even only 20–30% of cases are found to be cancer (Sickles, 1986). Thus decreasing the false-positive biopsy rate for mammographically detected abnormalities is important in image analysis of calcifications in mammograms. It also presents a challenge for radiologists who must not only recognise the presence of

MCCs, but also assess the likelihood of malignancy in order to avoid unnecessary biopsies (Lanyi, 1985).

The difficulties in MCCs diagnosis arise primarily in that the characteristic differences between benign and malignant lesions are subtle; some have drastic while some have similar appearances; some of the differences lie in the shape and curvature of individual blob of MCCs while some lie in the overall distribution of MCCs. Some experienced radiologists use considerable interpretive expertise to rate biopsy for those calcifications that are very unlikely to be malignant. However, for less trained radiologists, experiences come with extensive practices. One way to cope with this dilemma is to use a system to provide them with a second opinion to assist them in improvement upon diagnosis (Kegelmeyer et al., 1994).

The literature of classifying benign and malignant MCCs can be referred to the work proposed by Shen, Rangayyan, and Desautels (1994) in which the features, including moments, Fourier descriptors, and compactness, of selected

\* Corresponding author. Tel./fax: +886-6-275-7575.

E-mail addresses: pcchung@ee.ncku.edu.tw (P. Chung), cslo@neural.ee.ncku.edu.tw (C.S. Lo).

### Nomenclature

$\sigma$	variance used in the conditional probability density function
$\Psi$	defective degree of MCCs
$\bar{A}_B$	average size per blob
$A_c$	the number of pixels of MCCs
$A_R$	the area cover of MCCs
$C_1$	complex layer of first module
$C_2$	classification layer of second module
CP	compactness of MCCs
$d(\mathbf{x})$	Bayes classifier output when a pattern $\mathbf{x}$ is applied
$E$	elongation of MCCs
$f_c(\mathbf{x})$	the conditional probability density function of an $L$ -dimensional random vector $\mathbf{x}$ given that $\mathbf{x}$ belongs to class $c$
FN	the false negative rate
FP	the false positive rate
$h_{ij}$	the elevation of the pixel located at the $(i, j)$ position
$I$	irregularity of boundary of MCCs
$M_c$	circularity of MCCs
$M_d$	density of MCCs
$n$	the total number of MCCs test cases
$n_A$	number of patterns in class A
$N_B$	the number of blobs of MCCs
$n_B$	number of patterns in class B
$n_b$	the number of benign MCCs cases
$n_{bb}$	the number of benign cases classified correctly
$n_{bm}$	the number of benign cases classified incorrectly
$n_c$	number of patterns in a class $c$ where $c$ could denote A or B
$N_i$	the total number of pixels which form <i>shape feature dimension</i> $i$ in 3D figure layer within an ROI
$n_m$	the number of malignant MCCs cases
$n_{mb}$	the number of malignant cases classified correctly
$n_{mm}$	the number of malignant cases classified incorrectly
$N_\chi$	the summation of curvature number $\chi$
$R_b$	the rejection rate for benignancy
$R_m$	the rejection rate for malignancy
$S_1$	shape orientation layer of first module
$S_2$	feature formation layer of second module
$S_c$	the summation in the summation unit layer
$S_d$	scattering density of blobs within an ROI
TN	the true negative rate
TP	the true positive rate
$U_0$	input layer of S-Cognitron
$u(y)$	the unit step function, i.e. $u(y) = 1$ for $y = 0$ and $0$
$w_{mk}$	weights of training pattern unit layer
$\{\mathbf{x}_i^A\}_{i=1}^{n_A}$	$L$ -dimensional training pattern vectors belonging to class A
$\{\mathbf{x}_j^B\}_{j=1}^{n_B}$	$L$ -dimensional training pattern vectors belonging to class B
$x_{mk}^{n_c}$	an element in the input vector $x_k = (x_{1k}^{n_c}, x_{2k}^{n_c}, \dots, x_{N_k}^{n_c})^T$

blobs of clustered MCCs are computed. The report reveals that both true-positive fraction and true-negative fraction achieve 100% correct classification rate in leave-one-out tests. However, a clustered MCC usually consists of several blobs or scattered MCCs. Thus it is common to see some clustered MCCs from which it is impossible to select (or threshold) a blob. Furthermore, it is reported that the distribution pattern of MCCs determines the benignancy

and malignancy more than a specific blob within a clustered MCC, especially that most small blobs of malignant MCCs reveal like benignant. Therefore, it is highly suggested that a system for the classification of MCCs should take into considerations of both each individual blob and the group distribution.

Another difficulty arising in classifying benign and malignant MCCs is that the features of benign and

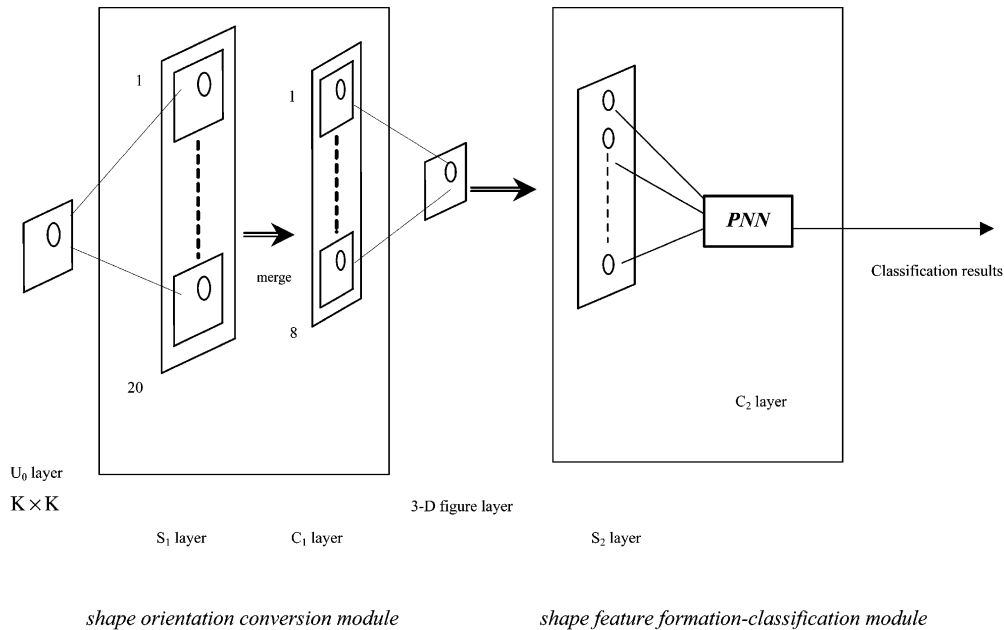


Fig. 1. Architecture of S-Cognitron.

malignant MCCs are far from specific that they cannot be described by some pre-selected shape patterns. According to literature reports, shape, curvature, and size are parts of basic characteristics in distinguishing benign and malignant MCCs. It was also reported that malignant MCCs are more likely to be irregular, granular, fine linear, and of small size while benign MCCs often have smooth boundary, popcorn-like, large rod-like, round, lucent-centred, eggshell, and are of large size. Even so, not only it is impossible to identify specific shape patterns which distinguish benign from malignant MCCs, one feature which plays major factor in the diagnosis in some cases might become irrelevant to the diagnosis of another case when some other features appear. It is also not uncommon to see contradict features co-exist in some cases. These factors cause the feature extraction difficult, if not impossible.

On the other hand, neural networks have been used in performing complex tasks. Among the existing neural network models, most of them such as the multilayer neural network, self-organised feature maps, associative memories, are designed based on minimizing a required equation. This approach does work fine in performing certain tasks, such as function approximation, minimal distance calculation for pattern classification, and optimisation problems. However, for performing visual task, as well as the classification of MCCs, this approach is far from sufficient. Another type of neural network model is the Fukushima's Neocognitrons (Fukushima, 1980, 1988; Fukushima & Miyake, 1982; Fukushima & Wake, 1991), and evolved Tricognitron (Xu, 1993; Xu & Chang, 1996). The Fukushima's Neocognitrons consist of feature extraction,  $S$ , layers and fusion,  $C$ , layers, where the  $S$  layers are constructed either by some pre-selected shape patterns, or by an unsupervised learning to code the object features in

the planes. The unsupervised Neocognitrons were considered comprising biological neural model, and effective to the recognition of characters, invariant to size, translation and handwriting (Fukushima, 1980, 1988; Fukushima & Miyake, 1982; Fukushima & Wake, 1991). Due to these characters of possessing biological meaning and effective in character recognition, the Neocognitrons were regarded one type of very unique neural models. But due to the uncertainty and complexity of MCCs' features related to benignancy and malignancy, the classification of MCCs using unsupervised Neocognitrons is not very successful. The contradict features co-exist in some cases usually cause the learning in the feature extraction difficult, if not possible, to converge for the Neocognitrons to achieve a high classification rate. On the other hand, as the shape patterns of the MCCs are far from specific to be pre-determined, the Neocognitrons using pre-selected shape coding do not work either. One alternative way adopted in the Shape Cognitron (S-Cognitron) is to use universal feature planes as opposed to use specific shape pattern planes or unsupervised learning in capturing features. Universal features are some basic low-order patterns which form the basic element of any shape patterns. In this paper, a S-Cognitron neural network, which is designed with universal feature planes, is proposed for classifying the benignancy and malignancy of MCCs. The S-Cognitron neural network serves as a fourfold operator, that is a feature extractor, displayer, selector as well as a classifier. Fig. 1 describes the structure of S-Cognitron, which consists of two modules, each of which has two layers. Between these two modules is an extra layer, called *3D figure layer*. The first module contains a shape orientation layer denoted by  $S_1$  and a complex layer denoted by  $C_1$ .  $S_1$  contains 20 cell planes of size  $N \times N$  representation of low level universal shape features obtained by

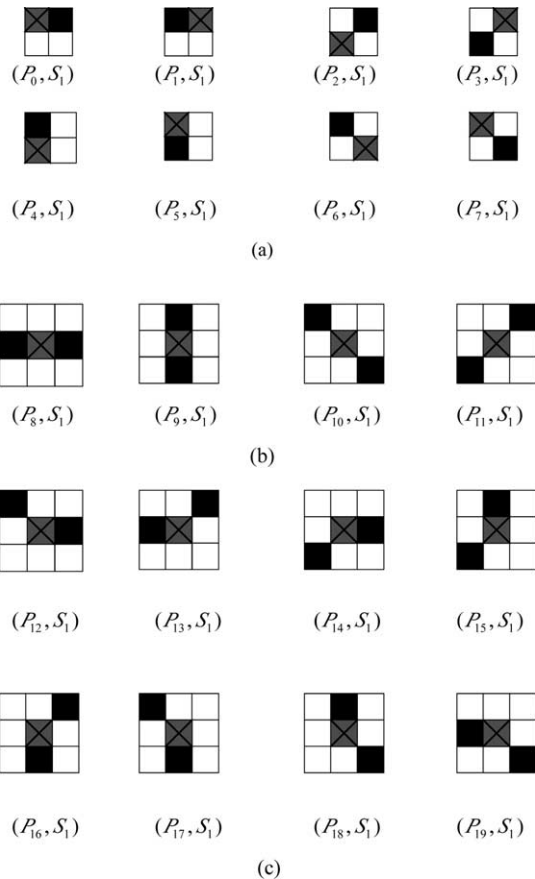


Fig. 2. (a) A set of eight  $2 \times 2$  spatial patterns which generate activity 1. (b) A set of four  $3 \times 3$  spatial patterns which generate activity 1. (c) A set of eight  $3 \times 3$  spatial patterns which generate activity 2.

using 20 window masks shown in Fig. 2.  $C_1$  contains eight cell planes merged from 20 cell planes of  $S_1$  representation of high level shape features. The task of the first module converts geometric shape orientations of an input pattern into numeric representations which are results of different activities generated by the window masking processing in  $S_1$  and merging procedure in  $C_1$ . The layer following the first module is 3D figure layer. It is a feature extraction-display layer, which extracts and represents the shape curvatures of an input pattern in terms of numeric representations. In the mean time, it also displays the input pattern as a 3D figure using these numeric representations as elevation of the pattern to show curvatures in the third dimension. The second module can be viewed as a joint feature formation and classification network and is made up of a feature formation layer,  $S_2$  which generates a desired set of shape features from the 3D figure layer, and a classification layer,  $C_2$  which employs a *probabilistic neural network* (PNN) (Specht, 1990) as a two-class (malignant and benign) classifier using the shape features produced by  $S_2$  as inputs. The classification performance of S-Cognitron is evaluated by Nijmegen mammogram database.

The remaining of the paper is organised as follows. Section 2 is devoted to S-Cognitron whose architecture is

delineated in detail. Section 3 focuses on the classification of MCCs. Section 4 includes results of classification performance of the designed system evaluated by the Nijmegen mammogram database. Final conclusions are given in Section 5.

## 2. Architecture of Shape Cognitron

As mentioned in Section 1, shape is one of major features in discriminating benignancy and malignancy of MCCs. To enable S-Cognitron to extract these shape features and, from which, to discriminate malignancy from benignancy, three major components are built inside the S-Cognitron. The first component consisting of  $S_1$  and  $C_1$  layers is a *shape orientation conversion module* which converts the shape orientation information from the input pattern to a numeric representation for each pixel and passes it on to the second component. The second component is a *shape curvature extraction-display layer*. It is a 3D figure layer which has only one  $N \times N \times 16$  cell cube. It displays a  $2D N \times N$  input pattern as a  $3D N \times N \times 16$  figure where the numeric value assigned to each pixel in the input pattern represents the shape curvature of that pixel. The numeral is generated by activities produced by the first module and can be viewed as the elevation of the pixel when the pattern is displayed as a 3D figure. The third component is a *shape feature formation-classification module* implemented by two layers, the feature formation layer,  $S_2$  and the classification layer,  $C_2$ . The task of layer  $S_2$  is to integrate and select shape curvatures obtained from the 3D figure layer, and generate a desired set of high-order shape features based on certain classification criteria. Layer  $C_2$  employs a PNN as a classifier to produce a final classification result. The details of each layer are described as follows.

### 2.1. Input layer $U_0$ of S-Cognitron

The input patterns to S-Cognitron are MCC's which are resulting from an MCCs detection system, for instance, the detection system described in (Chan, Lo, Sahiner, Lam, & Helvie, 1995; Dengler, Behrens, & Desaga, 1993; Liao et al., 1996; Wu, Doi, & Giger, 1992; Zhang et al., 1994) or any other CAD detection systems. The input pattern shows MCCs as a binary image corresponding to an ROI, which contains a cluster of MCCs. The prior information of an ROI includes the area of region over MCCs— $A_c$  and the number of blobs,  $N_B$ . The size of the input patterns in  $U_0$  is fixed at  $N \times N$ , where  $N$  in our system is 256, which is considered as the maximum size of a cluster of MCCs, and can vary subject to applications.

### 2.2. First module ( $S_1, C_1$ ) of S-Cognitron

This module can be thought of as a shape orientation conversion module, which converts shape orientations from









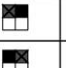
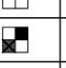
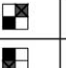
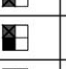
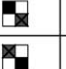
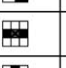
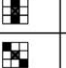
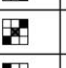
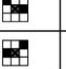
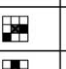
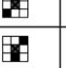
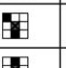
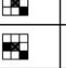
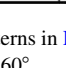
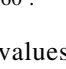
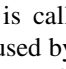
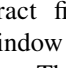
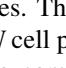
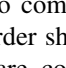
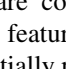
								
Shape Curvature	< 45°	45°	90°	135°	180°	225°	270°	360°
1		0	0	1	1	1	1	1
2		0	0	0	0	1	1	1
3		0	0	0	0	0	0	1
4		0	0	0	1	1	1	1
5		0	0	0	0	0	0	1
6		1	1	1	1	1	1	1
7		0	0	0	0	0	1	1
8		0	1	1	1	1	1	1
9		0	0	0	0	1	1	1
10		0	0	0	0	0	0	1
11		0	0	0	0	0	1	1
12		0	0	0	0	0	0	1
13		0	0	0	0	0	2	2
14		0	0	0	0	0	0	2
15		0	0	0	2	2	2	2
16		0	0	0	0	0	0	2
17		0	0	0	0	0	0	2
18		0	0	0	0	0	2	2
19		0	0	0	0	0	0	2
20		0	0	0	0	2	2	2

Fig. 3. Activities generated by spatial patterns in Fig. 2 to represent eight different geometric patterns, each of which corresponds to various curvatures, 22.5° (i.e. <45°), 45, 90, 135, 180, 225, 270, 360°.

input patterns into numeric values. Two layers are composed in this module. One is called  $S_1$  layer, where contains  $20 N \times N$  cell planes caused by 20 masks (see Fig. 2), which is designed to extract first-order shape of orientation features by three window masking processes built with universal feature planes. The other is called  $C_1$  layer, where contains eight  $N \times N$  cell planes obtained from  $S_1$  layer (see Fig. 4), which is to combine/fuse first-order shape orientations into second-order shape features. Please be noted that the orientations are computed on moving windows of specially designed feature masks. Thus the operation of S-Cognitron is essentially position and rotation invariant. As the obtained orientations are used to form high-order features in latter computation in which size normalisation is naturally imposed, the S-Cognitron is also scale-invariant.

### 2.2.1. Shape orientation layer $S_1$

This layer can be viewed as low-order shape orientation extraction layer, in which three sets of windows will be used to detect universal first-order features for input patterns.

Each window masking processing will result in a  $N \times N$  cell plane. Operations of the three sets of windows are described as follows.

(a) Eight  $2 \times 2$  windows denoted by  $(P_0, S_1)$ ,  $(P_1, S_1)$ ,  $(P_2, S_1)$ ,  $(P_3, S_1)$ ,  $(P_4, S_1)$ ,  $(P_5, S_1)$ ,  $(P_6, S_1)$ ,  $(P_7, S_1)$  as shown in Fig. 2(a) are used to match the horizontal orientation 0 and 180°, vertical orientation 90 and 270°, diagonal orientation 45 and 225°, and asymmetric diagonal orientation 135 and 315°. A cell marked by ‘X’ is the pixel currently being visited by a  $2 \times 2$  window and will be designated as a seed cell. A highlighted cell indicates a match between the window and the pattern while a blank cell showing ‘do not care’ during matching. If there occurs a match, the seed cell will be assigned an activity 1; 0, otherwise.

(b) Like  $2 \times 2$  windows, four  $3 \times 3$  windows denoted by  $(P_8, S_1)$ ,  $(P_9, S_1)$ ,  $(P_{10}, S_1)$ ,  $(P_{11}, S_1)$  shown in Fig. 2(b) are also used to match the horizontal orientation (0, 180°), vertical orientation (90, 270°), diagonal orientation (45, 225°) and asymmetric diagonal orientation (135, 315°). The difference from  $2 \times 2$  window masking lies in that the centre

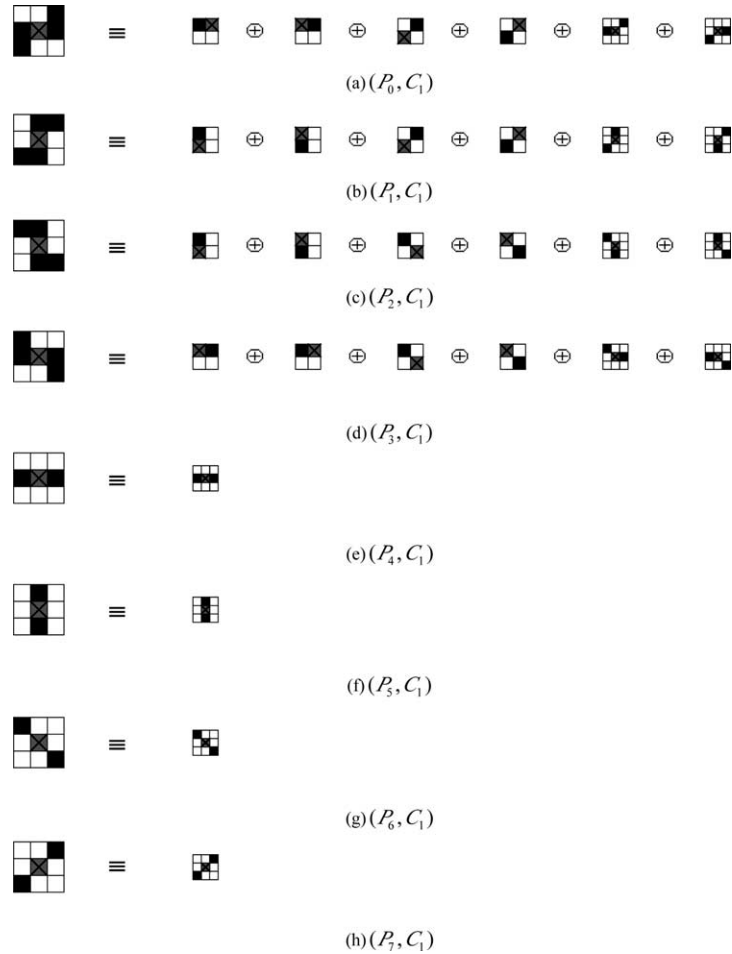


Fig. 4. The eight cell planes of complex layer  $C_1$  merged from 20 cell planes of simple layer  $S_1$ .

of the window is placed on the seed cell so that the pattern's orientation is across the seed cell; thus the  $3 \times 3$  windows are able to detect a second-order cell relation. If there is a match, the seed cell is assigned an activity 1; 0, otherwise.

(c) Eight  $3 \times 3$  windows denoted by  $(P_{12}, S_1)$ ,  $(P_{13}, S_1)$ ,  $(P_{14}, S_1)$ ,  $(P_{15}, S_1)$ ,  $(P_{16}, S_1)$ ,  $(P_{17}, S_1)$ ,  $(P_{18}, S_1)$ ,  $(P_{19}, S_1)$  shown in Fig. 2(c) are used to detect patterns with differences of  $22.5^\circ$ . Similar to the previously mentioned windows in Fig. 2(b), this eight windows are also used to detect second-order cell relations. But since this orientation difference  $22.5^\circ$  is more subtle than  $45^\circ$ , the seed cell is assigned an activity 2 if a match occurs; 0, otherwise.

As a result of using these 20 window masking processes, a total of 20  $N \times N$  cell planes will be generated, one for each window masking process. For demonstration, shown in Fig. 3 are the activities generated by spatial patterns in Fig. 2 to represent eight typical geometric patterns, each of which corresponds to various curvatures,  $22.5^\circ$  (i.e.  $< 45^\circ$ ),  $45$ ,  $90$ ,  $135$ ,  $180$ ,  $225$ ,  $270$ , and  $360^\circ$ .

### 2.2.2. Complex layer $C_1$

This layer can be viewed as a shape orientation fusion layer which combines the orientation information provided

by 20 cell planes in layer  $S_1$  and merges them into only eight cell planes:

- When two or more cell planes are merged into one cell plane, the activity assignment for this newly merged cell plane abides by *dominate-take-all* rule. More specifically, the activity of each pixel in the merged cell plane is assigned the largest activity among activities of the corresponding pixel in all cell planes to be merged.
- The six cell planes  $(P_0, S_1)$ ,  $(P_1, S_1)$ ,  $(P_2, S_1)$ ,  $(P_3, S_1)$ ,  $(P_{13}, S_1)$ ,  $(P_{14}, S_1)$  in layer  $S_1$  are merged into one cell plane, called  $(P_0, C_1)$  shown in Fig. 4(a).
- The six cell planes  $(P_2, S_1)$ ,  $(P_3, S_1)$ ,  $(P_4, S_1)$ ,  $(P_5, S_1)$ ,  $(P_{15}, S_1)$ ,  $(P_{16}, S_1)$  in layer  $S_1$  are merged into one cell plane, called  $(P_1, C_1)$  shown in Fig. 4(b).
- The six cell planes  $(P_4, S_1)$ ,  $(P_5, S_1)$ ,  $(P_6, S_1)$ ,  $(P_7, S_1)$ ,  $(P_{17}, S_1)$ ,  $(P_{18}, S_1)$  in layer  $S_1$  are merged into one cell plane, called  $(P_2, C_1)$  shown in Fig. 4(c).
- The six cell planes  $(P_0, S_1)$ ,  $(P_1, S_1)$ ,  $(P_6, S_1)$ ,  $(P_7, S_1)$ ,  $(P_{12}, S_1)$ ,  $(P_{19}, S_1)$  in layer  $S_1$  are merged into one cell plane, called  $(P_3, C_1)$  shown in Fig. 4(d).
- The four cell planes  $(P_8, S_1)$ ,  $(P_9, S_1)$ ,  $(P_{10}, S_1)$ ,  $(P_{11}, S_1)$  in layer  $S_1$  will not be merged but reassigned  $(P_4,$



Shape Curvature	< 45°	45°	90°	135°	180°	225°	270°	360°
	0	0	1	2	2	2	2	2
	1	1	1	1	1	1	2	2
	1	1	1	1	1	2	2	2
	0	1	1	1	2	2	2	2
	0	0	0	0	1	1	1	1
	0	0	0	0	0	0	1	1
	0	0	0	0	0	1	1	1
	0	0	0	0	0	0	0	1
3D-figures	2	3	4	5	7	9	b(11)	c(12)

Fig. 5. Numeric values of 3D figure layer generated by spatial patterns in Fig. 4 to represent eight different geometric patterns, each of which corresponds to various curvatures, 22.5° (i.e. <45°), 45, 90, 135, 180, 225, 270, 360°.

$C_1$ ), ( $P_5, C_1$ ), ( $P_6, C_1$ ), ( $P_7, C_1$ ), respectively, in layer  $C_1$  shown in Fig. 4(e)–(h).

The above merging processing produces a total of eight cell planes. For illustration, the eight typical patterns formed in layer  $C_1$  through merging basic universal features of  $S_1$  layer are shown in Fig. 5, where their activities in representing shape curvatures with  $0^\circ = 360, 45, 90, 135, 180, 225, 270$  and  $315^\circ$  are illustrated. However, it should be noted that the combination of the eight planes is sufficient to represent any second-order shape patterns.

### 2.3. 3D figure layer of S-Cognitron

This layer has only one  $K \times K$  cell plane resulting from summing up all eight cell planes in layer  $C_1$ . Since each

Table 1  
Shape curvatures (degree) generated by S-Cognitron

Shape curvature (°)	Curvature number
< 45	2
45	3
90	4
135	5
180	6, 7
225	8, 9
270	10, 11
$0^\circ = 360^\circ$	12

pixel in any cell plane has value either 0, 1, or 2, the summed cell plane will take integral values ranging from 0 to 16 which can be viewed as a numeric representation for the pixel. Representing numeric values, *curvature number* is called, as elevations of pixels can create a 3D figure for the input pattern where the third dimension may be called the *curvature dimension*. The elevation of pixels can show their shape curvatures in this shape feature dimension. Therefore, a  $K \times K$  pattern can be displayed by a 3D  $K \times K \times h$  figure where  $h \in \{0, 1, 2, \dots, 16\}$ . Because of that, this layer can be considered to be a shape curvature display layer. According to our experiments, activities 0 and 1 do not make any difference in recognition and therefore, they are merged to value 0 to accommodate 16 values (i.e. 2 bytes). The last row of Fig. 5 reveals the numeric representation of 3D figure layer for eight different patterns and Table 1 tabulates numeric representations obtained from 3D figures for eight different shape curvatures. Fig. 6 shows 3D figures produced in this layer for a number of clustered MCCs where the numeric value of each pixel in the pattern was obtained in accordance with the numeric representations of shape curvatures given in Table 1.

### 2.4. Second module ( $S_2, C_2$ ) of S-Cognitron

#### 2.4.1. Feature formation layer $S_2$

In order for S-Cognitron to produce an optimal feature set for classification, we follow the criteria proposed from

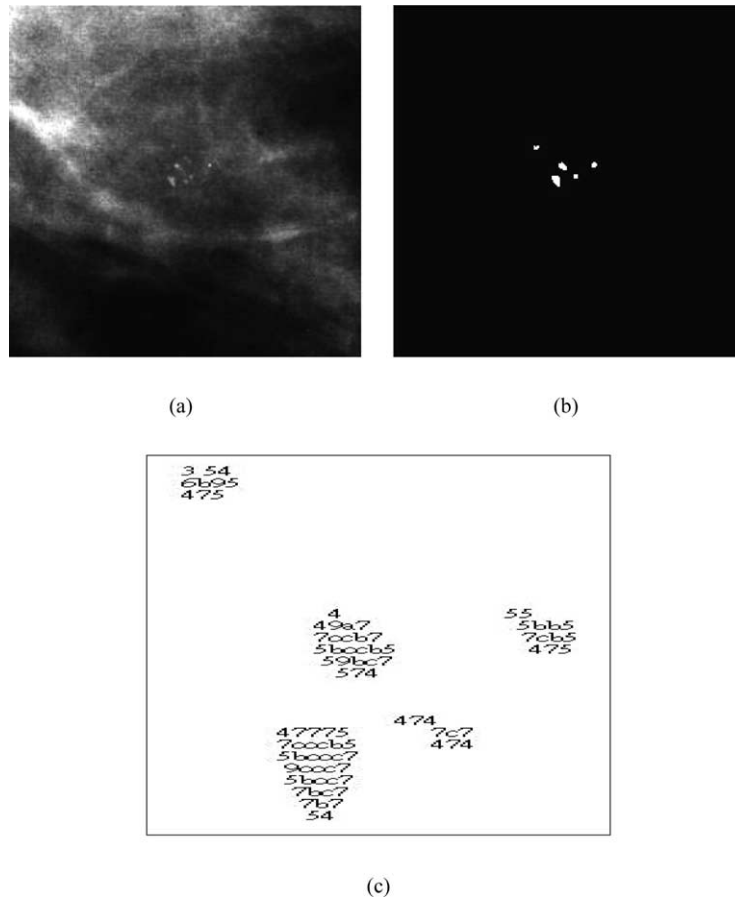


Fig. 6. (a) The original image of a cluster of microcalcifications. (b) The binary image of microcalcifications in (a). (c) The 3D figure of (b).

the Breast Imaging Reporting and Data System (BI-RADS) which was developed by the American College of Radiology (1993, 1995) and Lanyi (1986). These criteria are based on the numbers of MCCs, morphologic appearances, arrangements, concentrations, distributed sizes and densities, etc. Based on the guidelines, eight important shape features were generated in layer  $S_2$  from shape curvature and are tabulated in Table 2 (see Appendix A in detail). Different parameters were designed to generate the eight features by using summation of curvature numbers,

which are used to present the property of shape features properly, in this layer. The summation of curvature number  $\chi$ ,  $N_\chi$ , can be computed from the 3D figure pattern by the convolution formula  $N_\chi = \sum_{i=1}^K \sum_{j=1}^K [u(h_{ij} - \chi)]$  where  $h_{ij}$  is the elevation of the pixel located at the  $(i, j)$  position of the  $K \times K$  3D pattern and  $u(y)$  is the delta function, i.e.  $u(y) = 1$  for  $y = 0$  and 0, otherwise. For example, in the result of 3D figure layer shown in Fig. 6, the summation of curvature number 7 is computed as  $N_7 = \sum_{i=1}^K \sum_{j=1}^K [u(h_{ij} - 7)]$  and equal to 23.

Table 2  
Eight S-Cognitron generated features used for classification

Feature number	Feature characterisation	Formula
1	Average size per blob ( $\bar{A}_B$ )	$\bar{A}_B = A_c/N_B$
2	Scattering density of blobs within an ROI ( $S_d$ )	$S_d = N_B/A_R$
3	Density of MCCs ( $M_d$ )	$M_d = N_{12}/A_R$
4	Irregularity of MCCs ( $I$ )	$I = N_2 + N_3 + N_4$
5	Elongation of MCCs ( $E$ )	$E = N_5 + N_6 + N_7 + N_8 + N_9$
6	Circularity of MCCs ( $M_c$ )	$M_c = N_4 + N_5 + N_8 + N_9$
7	Compactness (CP)	$CP = P^2/N_B$
8	Defective degree ( $\Psi$ )	$\Psi = N_{10} + N_{11}$

Note: ROI, region of interest; MCCs, microcalcifications;  $A_c$ , the number of pixels of MCCs;  $A_R$ , the area cover of MCCs;  $N_B$ , the number of blobs;  $N_x$ , the total number of pixels of shape feature dimensional number no.  $x$  of 3D figure layer within an ROI.



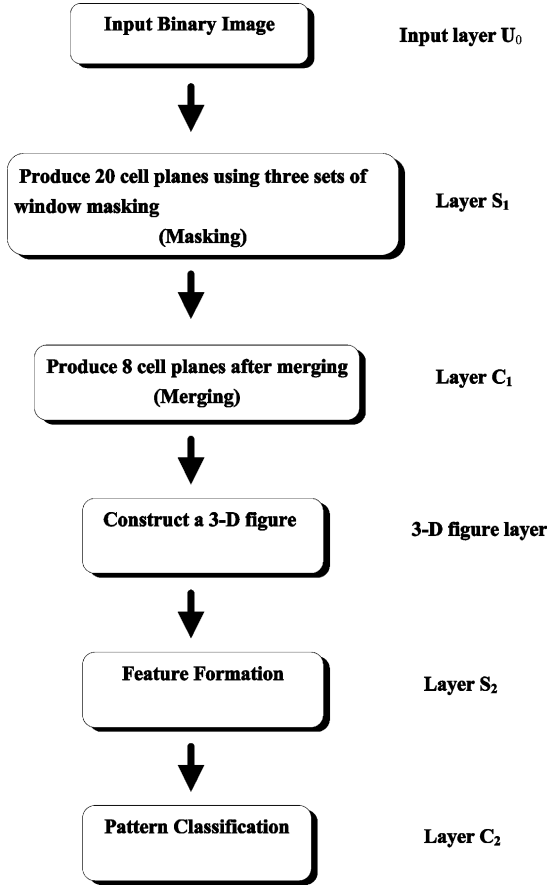


Fig. 7. Flow Chart of S-Cognitron.

#### 2.4.2. Classification layer $C_2$

This layer is regarded as a classification or recognition layer in which a PNN is implemented. Features generated in layer  $S_2$  are served as the inputs to the network. Through a statistical evaluation, the outputs provide the likelihood of malignance of MCCs associated with the input pattern. A more detailed description of this layer will be shown in Section 3.

In summary, how S-Cognitron works is described in the flow chart given in Fig. 7. It (1) first takes the detected MCCs produced by the MCC's detection system as input patterns in layer  $U_0$ , (2) uses the first module ( $S_1$ ,  $C_1$ ) to convert universal shape orientation information to numeric representations, (3) extracts and displays the numeric values in the curvature dimension in the 3D figure layer, (4) employs the second module ( $S_2$ ,  $C_2$ ) to format shape features in layer  $S_2$ , and finally (5) classifies MCCs in layer  $C_2$ .

### 3. Classification of MCCs in layer $C_2$

#### 3.1. Probabilistic neural networks

There are two reasons of choosing the PNN as a candidate for the classifier used in layer  $C_2$ . One is that unlike a multilayer perceptron with backpropagation which

requires long training time, a PNN requires much less training time to achieve Bayes classification. It also has generalisation ability and been proved to be successful in many classification problems. The other is that the output of a PNN can provide class estimates, which provide the likelihood of malignance for MCCs. Thus PNN can be very useful in medical diagnosis where likelihood values are more acceptable than yes–no results. The structure of a PNN is depicted in Fig. 8. In the PNN, there is an input layer, a hidden layer, a summation unit layer and an output layer where the hidden layer is also called the *training pattern unit layer* in the sense that each hidden node is represented by a training pattern. A brief description of PNN is given below.

Let  $\{\mathbf{x}_i^A\}_{i=1}^{n_A}$  and  $\{\mathbf{x}_j^B\}_{j=1}^{n_B}$  be  $L$ -dimensional training pattern vectors belonging to class A and class B, respectively, where  $n_A + n_B = n$ . Let  $f_c(\mathbf{x})$  be the conditional probability density function of an  $L$ -dimensional random vector  $\mathbf{x}$  given that  $\mathbf{x}$  belongs to class  $c$ . Then using *Parzen's windows method*, we can approximate  $f_c(\mathbf{x})$  by the following expression:

$$f_c(\mathbf{x}) \approx \frac{1}{(2\pi)^{L/2} \sigma^L} \left[ \frac{1}{n_c} \sum_{k=1}^{n_c} \exp \left\{ -\frac{(\mathbf{x} - \mathbf{x}_k^c)^T (\mathbf{x} - \mathbf{x}_k^c)}{2\sigma^2} \right\} \right] \quad (1)$$

where  $c = A$  or  $B$ .

If we assume that all sample vectors are normalised, i.e.  $\mathbf{x}^T \mathbf{x} = (x_k^{n_c})^T x_k^{n_c} = 1$  for  $n_c = n_A$  or  $n_B$  then based on Eq. (1) we can derive a Bayes classifier as follows:

$$d(\mathbf{x}) = n_A$$

$$\text{if } \frac{1}{n_A} \sum_{i=1}^{n_A} \exp \left\{ \frac{(\mathbf{x}^T \mathbf{x}_i^A - 1)}{\sigma^2} \right\} \geq \frac{1}{n_B} \sum_{i=1}^{n_B} \exp \left\{ \frac{(\mathbf{x}^T \mathbf{x}_i^B - 1)}{\sigma^2} \right\} \quad (2)$$

otherwise,  $d(\mathbf{x}) = n_B$ .

As a result, a neural network described in Fig. 8 can be used to implement Eq. (2), in such a way that the inner product,  $\mathbf{x}^T \mathbf{x}_k^{n_c}$  of the input vector  $\mathbf{x}$  with a training vector  $\mathbf{x}_k^{n_c}$  can be realised in the training pattern unit layer by setting weights  $w_{mk} = x_{mk}^{n_c}$  where  $x_k = (x_{1k}^{n_c}, x_{2k}^{n_c}, \dots, x_{N_k}^{n_c})^T$  (this operation is delineated by the rectangles in the network) and the summation

$$S_c = \frac{1}{n_c} \sum_{i=1}^{n_c} \exp \left\{ \frac{x^T x_i^c - 1}{\sigma^2} \right\} \quad (3)$$

in Eq. (3) can be realised in the summation unit layer by assigning 1 to weights going to the class to which the training vector belongs and 0, otherwise. The decision unit layer in the network is used to determine which class is supposed to be assigned to the input pattern. The desired class membership is the one which yields the maximum among outputs generated by the summation unit layer.

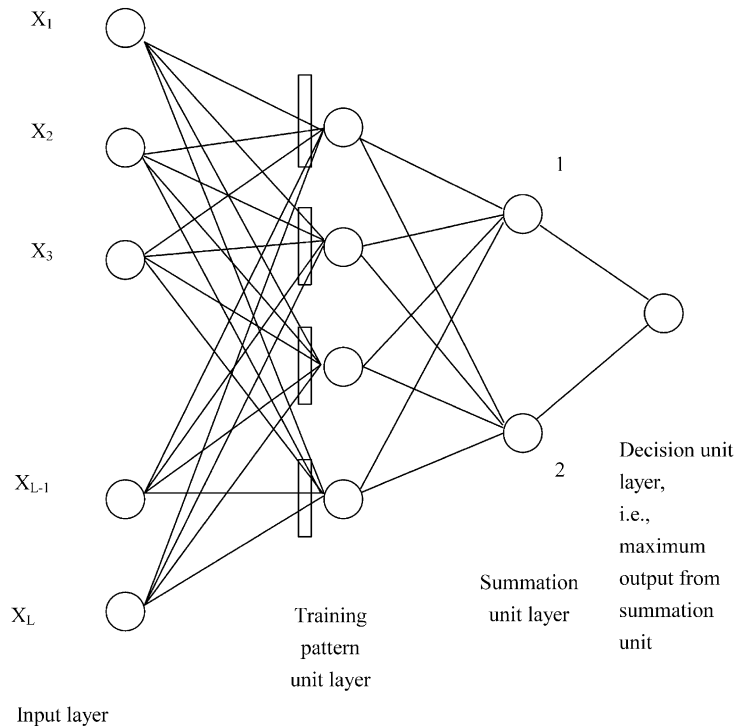


Fig. 8. Probabilistic neural network.

### 3.2. Classification of MCCs

The classification task presented in this section is accomplished by formatting shape features from  $S_2$  and feeding them to a PNN in layer  $C_2$ . All features in Table 2 will serve as an input set of the PNN in layer  $C_2$  for classification. The procedure in layer  $C_2$  can be described as follows:

1. There are eight nodes in the input layer to take shape features in Table 2.
2. The training pattern unit layer is made up of all training patterns which are 8D vectors, each having its own node. (Note that the weights from the input to the training pattern unit layer are fixed and determined by the associated training vector.)
3. The summation unit layer with weights determined by the classes to which the training vectors belong, in this case, only two classes, malignant and benign MCCs.

Table 3

Classification results using S-Cognitron are tabulated in benign cases and malignant cases

Benign MCCs (14 cases)			Malignant MCCs (36 cases)		
B	M	R	B	M	R
10	1	3	0	31	5

Total number: 50; B: benign; M: malignant; R: rejected.

4. The decision unit layer is the last layer that determines which class is the winner. The criterion is the maximum output of the summation unit layer.

## 4. Experiments

In this section, the 40-mammogram database provided by the Department of Radiology at the University of Hospital Nijmegen in Netherlands was used for experiments to evaluate the proposed system. There are 21 cases with seven cases being benign and 14 cases being malignant. One hundred and two ROIs were selected from these 40 mammograms, among which 29 ROIs are benign and 73 ROIs are malignant. The size of each ROI,  $N \times N$  is set to  $256 \times 256$ . From these selected 102 ROIs, 52 were randomly chosen for training cases (15 are benign and 37 are malignant) and the remaining 50 (14 are benign and 36 are malignant) for test cases. These sets of training patterns and test patterns were applied to the PNN in layer  $C_2$ . The parameter  $\sigma^2$  used in the PNN is set to 200.

Table 3 shows the classification results for the test cases in number of patterns. The rejection (R) in Table 3 represents that the case is undetermined when applied to the system and thus, no classification is made. This is primarily due to small probabilities generated in both classes, in which case, we would rather not make a decision. The classification rates of the result in Table 3 are shown in Table 4. Table 5 shows the classification rates when the rejection cases are excluded from our calculation.

Table 4  
Classification rates for Table 3

Classification rate (%)		
Correct	Incorrect	Rejected
82.0	2.0	16.0

Let  $n_{mm}$  and  $n_{bm}$  be the numbers of malignant cases classified correctly and benign cases classified incorrectly, respectively. Similarly,  $n_{bb}$  and  $n_{mb}$  are the numbers of benign cases classified correctly and malignant cases classified incorrectly, respectively. Let  $n_m$ ,  $n_b$  and  $n$  be the number of malignant MCC cases, the number of benign MCC cases, and the total number of MCC test cases. We can define the true positive rate by  $TP = n_{mm}/n_m$ , false positive rate by  $FP = n_{mb}/n_b$ , false negative rate by  $FN = n_{bm}/n_m$  and true negative rate by  $TN = n_{bb}/n_b$  where  $n_m = 36$  and  $n_b = 14$  in our experiments. Then the rejection rate for malignancy is  $R_m = (n - n_{mm} - n_{bm})/n$  and  $R_b = (n - n_{bb} - n_{mb})/n$  is the rejection rate for benignancy. In these rejection cases, we assume that doctors will encourage biopsy. In Table 6, TP, FP, TN, FN are also calculated where FN for the third feature set can reach 0% which means that it does not miss any true malignant MCC case in 36 malignant MCC test cases in spite of one false alarm (FP) case. It should be noted that if there is no rejection, that is,  $R_m = 0$  and  $R_b = 0$ , then  $TP + FN = 1$  and  $TN + FP = 1$ . Our experimental results also indicate that the proposed alternative approach, PNN-based classifier in S-Cognitron, produces encouraging performance in clustered MCC classification. Furthermore, because of the modular architecture, this network model can be easily modified/improved by replacing any plane with a better one in the future.

## 5. Conclusions

The classification of MCC's is one of the most difficult tasks encountered in computer aided diagnostic (CAD) systems. According to medical literatures, geometric patterns of clustered MCC's generally provide valuable information about differentiation between malignant and benign MCCs. In this paper, a new shape recognition-based neural network, S-Cognitron was designed and developed for the purpose of capturing geometric information of MCCs. The S-Cognitron built with universal feature planes is to convert the geometric curvature features of each pixel into

Table 5  
Classification rates with rejection ignored for Table 3

Classification rate (%)	
Correct	Incorrect
97.6	2.4

Table 6  
TP, FP, TN, FN rates for Table 3

TP	FP	TN	FN
86.1%	7.1%	71.4%	0.0%

numeric values by fusing first- and higher-order shape geometric features extracted by cascaded network layers. With this approach, geometric features can be extracted and displayed in a 3D figure as the elevation in the third dimension. The extracted features are fed into a classification layer for benign and malignance likelihood determination. Experimental results have shown that the proposed S-Cognitron neural network can effectively extract the geometrical features of MCCs. They also demonstrate the effectiveness of the extracted features in classifying benignancy and malignancy of MCCs.

Finally, it is worth mentioning that since the S-Cognitron uses universal feature planes in its front layers, it possesses the potential capability for the recognition of characters. However, the current version of S-Cognitron is not feasible for the recognition of characters, since its feature formation layer is designed only particularly for MCCs.

## Acknowledgements

This work was supported by National Science Council, Taiwan, ROC and Taichung Veterans General Hospital under Grants NSC88-2213-E-006-010 and TCVGH-885501D, respectively. We also thank for the 40-mammogram database provided by the Department of Radiology at the University of Hospital Nijmegen in Netherlands.

## Appendix A

BI-RADS is recommended by the American College of Radiology to standardise the language used in mammography reports. Calcifications in BI-RADS are interpreted in types and distribution. Types include coarse, large rod-like, round, lucent-centred, eggshell, milk of calcium, dystrophic, punctate, amorphous, pleomorphic, and fine linear calcifications; distributions are grouped, linear, segmental, regional, and scattered. Obviously, it is impossible to identify high level specific shape features for the type and distribution characteristics. In our approach, SCNN is used to construct these characteristics from integrating some low level universal patterns. In order to represent characteristics of types and distributions, eight features which contribute the maximum classification ability in discriminating benignancy and malignancy are selected by experiments. To form the eight features, the following prior information is required: the area cover of MCCs— $A_R$ , and the number of blobs— $N_B$ . The  $A_R$  is defined as the total area covered by

sets of  $32 \times 32$  windows which overlap with MCCs. Thus, it can be regarded as a loosely defined MCC area size. These two values can be easily obtained in the segmentation stage of MCCs. Let  $N_i$  be the total number of pixels which form shape feature dimension  $i$  in 3D figure layer within an ROI. Then, the eight features selected to represent types and distributions can be constructed from the outputs of 3D figure layer as follows:

1. *Average size per blob* ( $\bar{A}_B$ ): There are several blobs in a cluster of MCCs. A blob consists of MCC pixels which connected together. The average size of blobs is defined as  $\bar{A}_B = A_c/N_B$ , where  $A_c$  is the number of pixels of MCCs. This feature is used to represent the distributed types like *segmental*, *regional*, and *grouped*.
2. *Scattering density of blobs within an ROI* ( $S_d$ ):  $S_d = N_B/A_R$ . In this feature, it is useful to represent the distributed type like *scattered*.
3. *Density of MCCs* ( $M_d$ ):  $M_d = N_{12}/A_R$ , where no. 12 represents the nonboundary pixels of MCCs and  $N_{12}$  can be considered as the area of MCCs.
4. *Irregularity of boundary of MCCs* ( $I$ ): To evaluate calcifications like dystrophic, amorphous, and pleomorphic calcifications, irregularity of MCCs is an important clue to these features. Irregularity of MCCs are represented by nos. 2, 3, and 4 dependent on the curvature of shape. Therefore, it is defined by  $I = N_2 + N_3 + N_4$ .
5. *Elongation of MCCs* ( $E$ ): To evaluate calcifications like large rod-like and fine linear calcifications, the elongation of MCCs is an important clue to these features. In our observation, elongation of MCCs is associated with nos. 5–9. Therefore, elongation of MCCs is defined as  $E = N_5 + N_6 + N_7 + N_8 + N_9$ .
6. *Circularity of MCCs* ( $M_c$ ): To evaluate calcifications like round, lucent-centred, and eggshell calcifications, circularity of MCCs is an important clue to these features. In our observation, circularity of MCCs is associated with nos. 4, 5, 8, and 9. Therefore, circularity of MCCs is defined as  $M_c = N_4 + N_5 + N_8 + N_9$ .
7. *Compactness* (CP): The boundary pixel of blobs is represented in nos. 2–9 of the shape feature dimensional number. Therefore, it is reasonable to define the perimeter of blobs  $P = \sum_{i=2}^9 N_i$ . Then, the compactness is defined as  $CP = P^2/N_B$ .
8. *Defective degree* ( $\Psi$ ): The zigzag boundary of a round MCC is also the measured score of classifications, called defective degree, in the paper. Nos. 10 and 11 always occur on the cave of the corner. They are used to measure the defective degree of MCCs. The defective degree  $\Psi = N_{10} + N_{11}$ .

## References

- American College of Radiology (1993). *Breast imaging reporting and data system (BI-RADS)*. Reston, VA: American College of Radiology.
- American College of Radiology (1995). *Breast imaging reporting and data system (BI-RADS)* (2nd ed.). Reston, VA: American College of Radiology.
- Chan, H. P., Lo, S. C., Sahiner, B., Lam, K. L., & Helvie, M. A. (1995). Computer-aided detection of mammographic microcalcifications: Pattern recognition with an artificial neural network. *Medical Physics*, 22, 1555–1567.
- Dengler, J., Behrens, J., & Desaga, J. F. (1993). Segmentation of microcalcifications in mammograms. *IEEE Transactions on Medical Imaging*, 12(4), 634–642.
- Fukushima, K. (1980). Neocognitron: A self-organizing neural network model for a mechanism of pattern recognition unaffected by shift in position. *Biological Cybernetics*, 36, 193–202.
- Fukushima, K. (1988). Neocognitron: A hierarchical neural network capable of visual pattern recognition. *Neural Networks*, 1, 119–130.
- Fukushima, K., & Miyake, S. (1982). Neocognitron: A new algorithm for pattern recognition tolerant of deformations and shift in position. *Pattern Recognition*, 15, 455–469.
- Fukushima, K., & Wake, N. (1991). Handwritten alphanumeric character recognition by the neocognitron. *IEEE Transactions on Neural Networks*, 2, 355–365.
- Kegelmeyer, M. P., Pruneda, J. M., Bourland, P. D., Hillis, A., Riggs, M. W., & Nipper, M. L. (1994). Computer-aided mammographic screening for spiculated lesions. *Radiology*, 191, 331–337.
- Lanyi, M. (1985). Microcalcifications in the breast—A blessing or a curse? *Diagnostic Image Clinical Medicine*, 54, 126–145.
- Lanyi, M. (1986). *Diagnosis and differential diagnosis of breast calcifications*. Berlin: Springer, pp. 91–107.
- Liao, P. S., Hsu, B. C., Lo, C. S., Chung, P. C., Chen, T. S., Lee, S. K., Cheng, L., & Chang, C. I. (1996). Automatic detection of microcalcifications in digital mammograms by entropy thresholding. *Proceedings of the IEEE International Conference in Medicine and Biology Society* (pp. 1075–1076).
- Shen, L., Rangayyan, R. M., & Desautels, J. E. L. (1994). Application of shape analysis to mammographic calcifications. *IEEE Transactions on Medical Imaging*, 13, 263–274.
- Sickles, E. A. (1986). Breast calcifications: Mammographic evaluation. *Radiology*, 160, 289–293.
- Specht, D. F. (1990). Probabilistic neural network. *Neural Networks*, 3, 109–118.
- Wu, Y., Doi, K., Giger, M. L., & Nishikawa, R. M. (1992). Computerized detection of clustered microcalcifications in digital mammograms: Applications of artificial neural networks. *Medical Physics*, 19(3), 555–560.
- Xu, Y. (1993). Tricognitron: A new approach to handwritten alphanumeric character recognition. MS Thesis, Department of Electrical Engineering, University of Maryland Baltimore County, Baltimore, MD.
- Xu, Y., & Chang, C. I. (1996). Implementation of a 3-D model for neocognitron. *Proceedings of International Conference in Neural Network*, Washington, DC, June 3–6 (pp. 794–799).
- Zhang, W., Doi, K., Giger, M. L., Wu, Y., Nishikawa, R. M., & Schmidt, R. A. (1994). Computerized detection of clustered microcalcifications in digital mammograms using a shift-invariant artificial neural networks. *Medical Physics*, 21(4), 517–524.